Basic Theory and Experiment Study on New Electro-hydraulic Exciter

Dong Han, Guofang Gong, Yi Liu and Huayong Yang

The State Key Lab of Fluid Power Transmission and Control, Zhejiang University, Hangzhou, China
E-mail: juebuqingchen@gmail.com, gfgong@zju.edu.cn, 8303446@qq.com, yhy@zju.edu.cn

Abstract

As important special engineering equipment, tamper is used to complete the work of construction and maintenance in the railway field. In the present market, tampers are mostly mechanically driven and exist technical limitations. A new electro-hydraulic exciter applied on new tamper is proposed. It is mainly composed of new spin valve and new micro-displacement oscillation cylinder. In the paper, new model of spin valve orifice is established based on FLUENT simulation. Theoretical model of exciter is established to early explore the relationship between structure parameters and performance parameters. Experiments are conducted to validate theoretical results. The results show that new model of spin valve and theoretical model of exciter are both accurate. New exciter can realize the flexible adjustment of amplitude and frequency. Therefore, design of new tamper is reasonable and it adapts to all kinds of complex working conditions including hardened ballast and loose ballast. The paper adopts methods of combinations among simulation analysis, theoretical model and testing. The research is very significant and provide theoretical and practical direction for design and optimization of electro-hydraulic exciter.

Keywords: tamper, electro-hydraulic exciter, simulation analysis, spin valve port, theoretical model

1 Introduction

With the rapid development of railway transport systems and the improvement of people's living standard, requests for comfort and safety by train are growing. So demands of routine maintenance have been considerably growing[1-2]. As large track maintenance machinery, tamping vehicle can obviously improve security, reliability and comfort of high-speed trains. As core equipment of tamping vehicle, the tamper, based on the principle of clamping and vibrating, changes ballast's original permutation and drives them to flow under the sleeper evenly and compactly [3-4]. As we all know, track environment is complex and variable, so it requires tamper having strong adaptability to different working conditions through different kinds of vibration. Vibration with high frequency and low amplitude is fit for hardened ballast. Vibration with low frequency and high amplitude is fit for loose ballast [5].

The current market of tamper is mostly taken by Hasco(America), Matisa(Switzerland) and Plasser(Austria). With multi-functions and high efficiency, their structures are different. Hasco's tamper has a horizontal twisting movement through eccentric linkage[6-8]. Matisa's tameper has a vertical elliptical movement through eccentric linkage[9-11]. and Plasser's tamper has a swing movement through eccentric linkage[12-14]. Therefore, they all use eccentric shaft to realize mechanical vibration[15-16], which has some technical limitations as follows. First, because of fixed waveform, amplitude and frequency, they can't satisfy complex and variable track conditions. Then, some don't have independent tamping arms, which leads to inconvenience in repair. What's more, mechanical vibration of eccentric linkage accelerates wear.

Compared to tampers of mechanical vibration, hydraulic vibration has advantages of stepless speed, flexible load etc. Therefore, a new tamper of hydraulic vibration(Patent No.: 201010104672.9) is represented. It has independent relationship between squeeze motion and vibration motion. As key parts, a new electro-hydraulic exciter(Patent No.: 201010520147.5) is also presented. It mainly consists of spin valve(Patent No.: 201010100305.1) and micro-displacement oscillation cylinder(Patent No.: 201110229924.5).

The paper introduces working principle of new tamper and electrohydraulic exciter. FLUENT simulation of spin valve orifice indicates special features of spin valve orifice. Based on simulation analysis, revised theoretical model of spin valve port is established. In accordance with numerical analysis, the characteristics and performances of the electro-hydraulic exciter are early explored. At last, experiments results helps validate model and optimize design.

2 Operating principle

2.1 Principle of new tamper

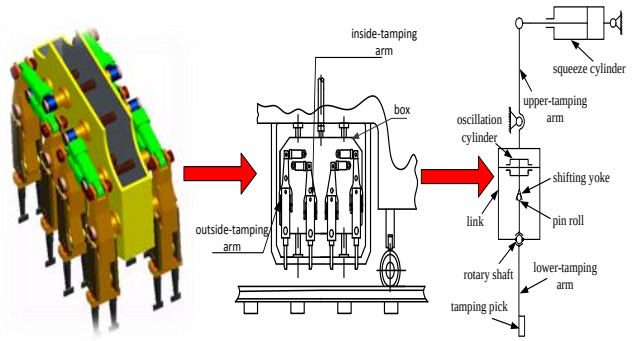

Figure 1: Operating principle of new tamper

As shown in fig.1, the new tamper is composed of box and four same pairs of independent tamping arms, including outside-tamping arms and inside-tamping arms. The box and upper-tamping arm are both hinged with the squeeze cylinder, which controls the upper-tamping arm's squeeze motion. The upper-tamping arm and lower-tamping arm are connected through the link. In addition, the tamping pick and pin roll are fixed on two ends of the lower-tamping arm separately. The vibration cylinder and shafting yoke are joined into a unit, which impels the lower-tamping arm to swing around the rotary shaft through shafting yoke in order to achieve high frequency vibration.

2.2 Principle of new exciter

As shown in Figure 2, new electro-hydraulic exciter is made up primarily of rotary valve and micro-displacement double-functioned hydraulic cylinder. In the new designed tamping device [15], the load that shifting yoke drives the lower-damping arm to swing through the rotary shaft is replaced by the load that cylinder body drives the mass to reciprocate on the linear guide rail. The rotary spool which is driven by step motor has two shoulders with the same structure. There are some rectangle grooves on the shoulder, and also the same number of corresponding rectangle windows in the sleeve. The hydraulic cylinder is driven by the rotary valve. As the piston is fixed with moving body, the main oil channel is designed in the piston rod, check valve lying at the end of main channel. There is an inner-leakage channel in the sidewall of body with the renewable damping hole. Besides, with the requirement of micro-displacement, some unique limit holes linked to main channel are applied to achieve automatic displacement limit but also to avoid collision between piston and end cap.

When the step motor impels spool to an specific angle, oil flows from port P to port A, through the main channel, through the right check valve, then through the right check valve and the right limit holes. At the same time, oil flows through left limit holes, through main channel, then from port B to port T. In this case, the cylinder body moves right and gets the outer load to vibrate right. When the step motor impels spool to another angle, similar with the above mentioned, oil flows from port P to port B and from port A to port T. In this case, the cylinder body moves left and gets the outer load to vibrate left. With the change of step motor's speed, the frequency of rotary spool changes leading to the changes of cylinder's working frequency.

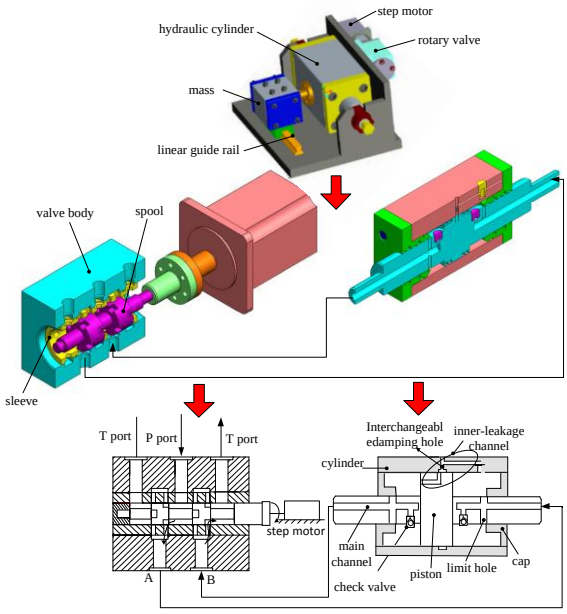

Figure 2: Operating principle of new exciter

The performance comparison of different tamping devices is shown in Table 1. Combined with the Figure 1, Figure 2 and Table 1, we can conclude that the new tamping device has great advantage in excitation since the flexible adjustment of frequency and amplitude can satisfy all kinds of complex working condition.

Table 1 Performance comparison of different tamping devices

Tamping machine	Plasser	Harsco	Matisa	New
Shock mechanism quantity	2	8	2	16
Relevant tamping arms quantity	8	2	8	1
Vibration frequency(Hz)	35	53	45	Adjustable
Amplitude	Fixed	Fixed	Fixed	Adjustable

3 CFD simulation of orifice

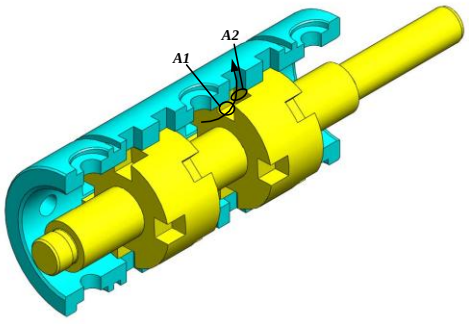

Figure 3: Structure of spool and sleeve

Figure 3 presents the structure of spool and sleeve. Four same rectangle grooves are distributed evenly on each side of every shoulder. Every groove's central angle is 22.5° and central angle of two neighbor grooves is 90° . Figure 4 is the flow field model of inlet orifice. Because of its complex, flexible unstructured mesh is adopted. Figure 5 illustrates the inlet orifice with about 120000 tetrahedron meshes.

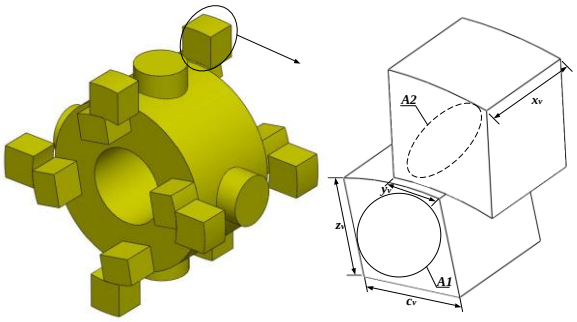

Figure 4: Flow field model of inlet orifice

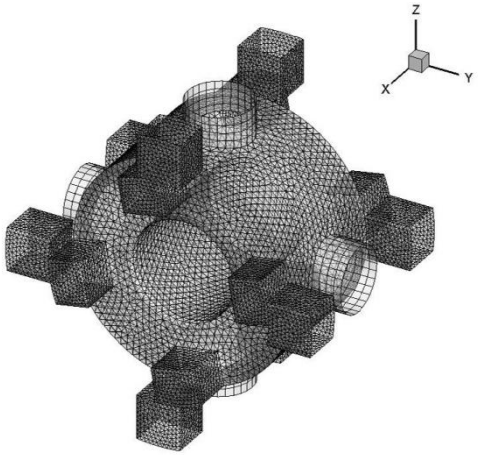

Figure 5: Flow field model of inlet orifice with meshes

Before the dynamic simulation, boundary conditions and initial conditions are set as follows. Assuming that oil is regarded as incompressible and its gravity is negligible. Oil density is 889 kg/m^3 and kinematic viscosity is about 4×10^{-5} m^2/s. The boundary conditions of inlet and outlet are the very pressure boundary conditions. Considering the dramatic changes in flow field, k-ζ turbulent model is adopted.

Assuming that it's zero opening when the angular displacement is at θ=0° , Figure 6 shows inlet orifice's pressure distribution under different angular displacement of 12° , 22.5° and 33° . In Figure (a) and (b), when the angular displacement is at θ=12° , the opening is also at 12° with a bigger tendency. Pressure drop is mainly concentrated on *A1* and *A2* surface. In Figure (c) and (d), when the angular displacement is at θ=22.5° , the opening is largest at 22.5° . Pressure drop is also concentrated on *A1* and *A2* surface, but in less extent than that in Figure (a) and (b). In Figure (e) and (f), when the angular displacement is at θ=33° , the opening is at 12° with a smaller tendency. Pressure drop is also concentrated on *A1* and *A2* surface in equal extent compared with Figure (a) and (b). According to the above analysis, conclusion can be made that pressure drop is mainly concentrated on *A1* and *A2* surface. With a rise of orifice opening, unchangeable A1 and bigger *A2* made the pressure distribution change. As consequence, pressure drop is less concentrated. Therefore, the rotary valve orifice exists the two throttles phenomena.

4 Analysis of mathematic modeling

4.1 Flow area model of rotary valve orifice

According to the above dynamic simulation, the two throttles phenomenon happened in the orifice. Therefore, the flow area model of orifice is established based on the two throttles phenomenon. Combined with conduction relationship shown in Figure 3 and geometrical relationship shown in Figure 4, flow area of *A1* surface doesn't vary with the spool rotation and can be written as

$$A_{1i}=\frac{\pi r^2}{16}-r^2\sin\frac{\pi}{16}\cos\frac{\pi}{16}+2rz_v\sin\frac{\pi}{16} \tag{1}$$

Where z_v is the radial length of orifice.

Flow area of *A2* surface varies periodically with the spool rotation. So it can be describes as

$$A_{2i}(i=1,4)=\begin{cases} x_v r\theta & \theta\in\left[\frac{n\pi}{2},\frac{(4n+1)\pi}{8}\right) \\ \frac{\pi x_v r}{4}-x_v r\theta & \theta\in\left[\frac{(4n+1)\pi}{8},\frac{(4n+2)\pi}{8}\right) \\ 0 & \theta\in\left[\frac{(4n+2)\pi}{8},\frac{(4n+3)\pi}{8}\right) \\ 0 & \theta\in\left[\frac{(4n+3)\pi}{8},\frac{(n+1)\pi}{2}\right) \end{cases} \tag{2}$$

$$A_{2i}(i=2,3)=\begin{cases} 0 & \theta\in\left[\frac{n\pi}{2},\frac{(4n+1)\pi}{8}\right) \\ 0 & \theta\in\left[\frac{(4n+1)\pi}{8},\frac{(4n+2)\pi}{8}\right) \\ x_v r\theta-\frac{\pi x_v r}{4} & \theta\in\left[\frac{(4n+2)\pi}{8},\frac{(4n+3)\pi}{8}\right) \\ x_v r\theta-\frac{\pi x_v r}{2} & \theta\in\left[\frac{(4n+3)\pi}{8},\frac{(n+1)\pi}{2}\right) \end{cases} \tag{3}$$

Taking into the two throttles phenomenon into account, the flow area of orifice is calculated in accordance with series connection between *A1* surface and *A2* surface. So the relation among pressure drop of orifice Δp_i, pressure drop of *A1* surface Δp_{1i} and pressure drop of *A2* surface Δp_{2i} is given as

$$\Delta p_i=\Delta p_{1i}+\Delta p_{2i} \tag{4}$$

The flow equation through the orifice is shown as

$$q_i = C_d A_i \sqrt{2\Delta p_i / \rho} \tag{5}$$

Where C_d is flow rate coefficient, ρ is oil density.

The flow equation through *A1* surface is shown as

$$q_{1i} = C_d A_{1i} \sqrt{2\Delta p_{1i} / \rho} \tag{6}$$

The flow equation through *A2* surface is shown as

$$q_{2i} = C_d A_{2i} \sqrt{2\Delta p_{2i} / \rho} \tag{7}$$

Because of series connection between *A1* surface and *A2* surface, $q_i=q_{1i}=q_{2i}$. Thus, based on the above analysis equations, the flow area of all orifices is calculated as

$$A_v = \frac{4}{\sqrt{1/A_{1i}^2 + 1/A_{2i}^2}} = \begin{cases} \dfrac{4}{\sqrt{\dfrac{1}{\left(\dfrac{\pi r^2}{16} - r^2 \sin\dfrac{\pi}{16}\cos\dfrac{\pi}{16} + 2rz_v \sin\dfrac{\pi}{16}\right)^2} + \dfrac{1}{(x_v r\theta)^2}}} & \theta \in \left[\dfrac{n\pi}{2}, \dfrac{(4n+1)\pi}{8}\right) \\ \dfrac{4}{\sqrt{\dfrac{1}{\left(\dfrac{\pi r^2}{16} - r^2 \sin\dfrac{\pi}{16}\cos\dfrac{\pi}{16} + 2rz_v \sin\dfrac{\pi}{16}\right)^2} + \dfrac{1}{\left(\dfrac{\pi x_v r}{4} - x_v r\theta\right)^2}}} & \theta \in \left[\dfrac{(4n+1)\pi}{8}, \dfrac{(4n+2)\pi}{8}\right) \\ \dfrac{4}{\sqrt{\dfrac{1}{\left(\dfrac{\pi r^2}{16} - r^2 \sin\dfrac{\pi}{16}\cos\dfrac{\pi}{16} + 2rz_v \sin\dfrac{\pi}{16}\right)^2} + \dfrac{1}{\left(x_v r\theta - \dfrac{\pi x_v r}{4}\right)^2}}} & \theta \in \left[\dfrac{(4n+2)\pi}{8}, \dfrac{(4n+3)\pi}{8}\right) \\ \dfrac{4}{\sqrt{\dfrac{1}{\left(\dfrac{\pi r^2}{16} - r^2 \sin\dfrac{\pi}{16}\cos\dfrac{\pi}{16} + 2rz_v \sin\dfrac{\pi}{16}\right)^2} + \dfrac{1}{\left(x_v r\theta - \dfrac{\pi x_v r}{2}\right)^2}}} & \theta \in \left[\dfrac{(4n+3)\pi}{8}, \dfrac{(n+1)\pi}{2}\right) \end{cases} \tag{8}$$

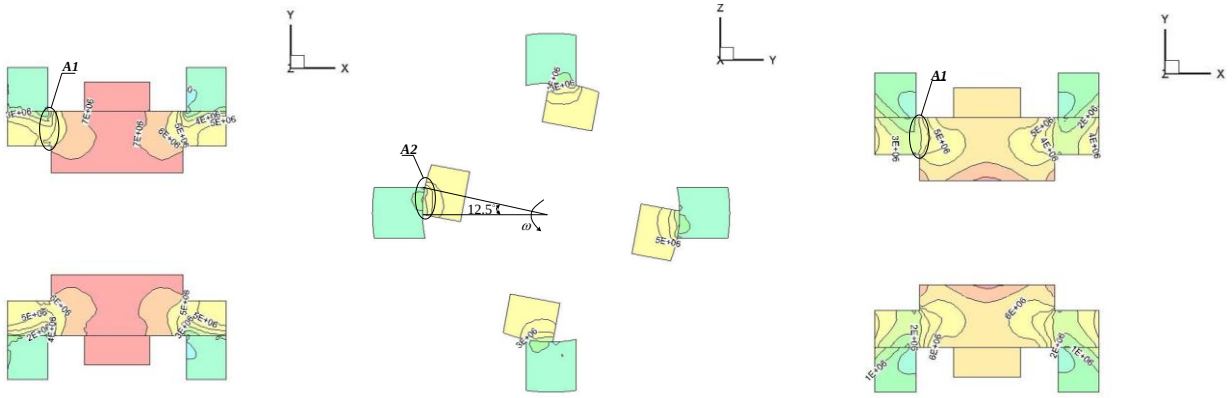

(a) Pressure distribution in Z plane, θ=12° (b) Pressure distribution in X plane, θ=12° (c) Pressure distribution in Z plane, θ=22.5°

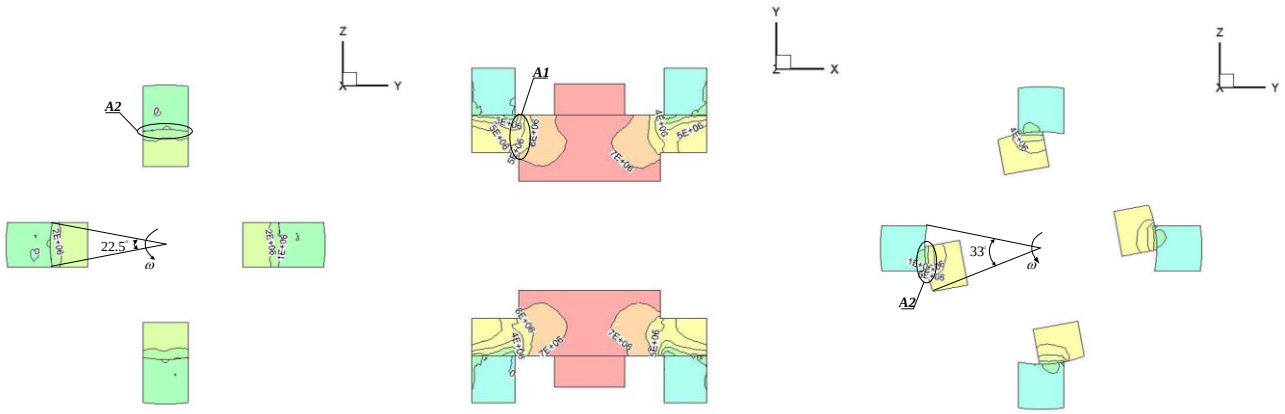

(d) Pressure distribution in X plane, θ=22.5° (e) Pressure distribution in Z plane, θ=33° (f) Pressure distribution in X plane, θ=33°

Figure 6 Pressure distribution of inlet orifice

4.2 Modeling of hydraulic exciter

The Principle of new electro-hydraulic exciter is shown in Figure 7. It is assumed that the system pressure p_s is constant, the total supply flow is q_{vs}, the flow through the load is q_{vl} and the pressure drop across the load is p_l.

If the orifices are both matched and symmetrical, the flows in diagonally opposite arms of the bridge in Figure 7 are equal. The area of valve port is A_v. Therefore, $A_{v1} = A_{v3}$, $A_{v2} = A_{v4}$. Supposing the rotation period of valve spool is T, the equations of flow through the orifices are shown as follows:

For $0 \le t \le \frac{T}{8}, \frac{T}{4} \le t \le \frac{3T}{8}, \frac{T}{2} \le t \le \frac{5T}{8}, \frac{3T}{4} \le t \le \frac{7T}{8}$,

$$\begin{cases} q_{v1} = q_{v3} = C_d A_{v1} \sqrt{\dfrac{2(p_s - p_1)}{\rho}} = C_d A_{v1} \sqrt{\dfrac{p_s - p_l}{\rho}} \\ q_{v2} = q_{v4} = 0 \end{cases} \tag{9}$$

For $\frac{T}{8} \le t \le \frac{T}{4}, \frac{3T}{8} \le t \le \frac{T}{2}, \frac{5T}{8} \le t \le \frac{3T}{4}, \frac{7T}{8} \le t \le T$,

$$\begin{cases} q_{v1} = q_{v3} = 0 \\ q_{v2} = q_{v4} = C_d A_{v2} \sqrt{\frac{2p_1}{\rho}} = C_d A_{v2} \sqrt{\frac{p_s + p_l}{\rho}} \end{cases} \tag{10}$$

Where C_d is flow rate coefficient; ρ is oil density; p_1, p_2 are pressure of hydraulic cylinder two cavity respectively.

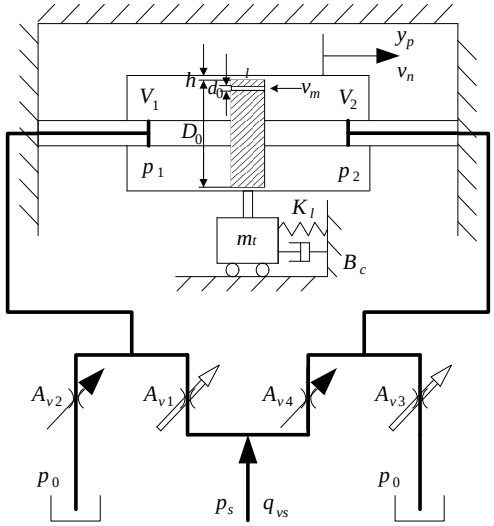

Figure 7 The principle of new electro-hydraulic exciter

The flow rate continuity equation of the left chamber of the cylinder.

$$q_{v1} - q_{v2} = \frac{dy_p}{dt} A_p + \frac{V_1}{\beta_e} \frac{dp_1}{dt} + C_{ep} p_1 + q \tag{11}$$

The flow rate continuity equation of the right chamber of the cylinder.

$$q_{v3} - q_{v4} = \frac{dy_p}{dt} A_p - \frac{V_2}{\beta_e} \frac{dp_2}{dt} - C_{ep} p_2 + q \tag{12}$$

Where y_p is displacement of cylinder; β_e is effective bulk modulus of oil; A_p is area of piston; V_1 is volume of forward chamber, $V_1 = V_{o1} + A_p y_p$, V_{o1} is initial volume of forward chamber; V_2 is volume of return chamber, $V_2 = V_t - (V_{o1} + A_p y_p)$, V_t is total volume of cylinder chamber; C_{ep} is the coefficient of external leakage; q is the internal leakage flow.

If external leakage is zero, the relationship between the load flow of the cylinder is $q_{vl} = q_{v1} - q_{v2}$.

That is,

$$\begin{aligned} q_{vl} &= \text{sign}(\frac{\pi}{4} - 2\pi ft) A_v \frac{C_d}{\sqrt{\rho}} \sqrt{p_s - \text{sign}(\frac{\pi}{4} - 2\pi ft) p_l} \\ &= \begin{cases} C_d A_{v1} \sqrt{\frac{p_s - p_l}{\rho}}, & (0 \le t \le \frac{T}{8}); \\ C_d A_{v2} \sqrt{\frac{p_s + p_l}{\rho}}, & (\frac{T}{8} \le t \le \frac{T}{4}). \end{cases} \end{aligned} \tag{13}$$

General hydraulic system is low damping, increasing hydraulic damping can improve the vibration system performance[17]. Its method is mainly through the interchangeable damping hole in the cylinder barrel to get different damping as shown in Figure 3. Damping hole flow of flow equation is

$$q = A_p v_p = A_p \frac{dy_p}{dt} \tag{14}$$

Where v_p is speed of cylinder.

The average flow velocity of damping hole is

$$v_d = \frac{4q}{\pi d_0^2} = \frac{4A_p}{\pi d_0^2} \frac{dy_p}{dt} \tag{15}$$

Flow makes pressure difference of hydraulic cylinder two cavity. According to the laminar flow pressure loss formula, the equation of pressure difference of hydraulic cylinder two cavity is :

$$p_{l1} = \lambda \frac{l}{d_0} \frac{\rho v_d^2}{2} \tag{16}$$

Where λ is resistant coefficient of pipe, $\lambda = \frac{75}{R_e}$, R_e is reynolds number, $R_e = \frac{v_d d_0}{\upsilon}$, υ is kinematic viscosity; d_o is diameter of interchangeable damping hole; l is the Piston long.

That is,

$$p_{l1} = R_1 A_p \frac{dy_p}{dt} \tag{17}$$

Where R_1 is flowing resistance, $R_1 = \frac{150\mu l}{\pi d_0^4}$; μ is absolute viscosity, $\mu = \upsilon\rho$.

The force of the damping hole effect is

$$F_1 = B_1 \frac{dy_p}{dt} \tag{18}$$

Where $B_1 = R_1 A_p^2$ is damping coefficient.

Oil can also produce damping effect through the gap between cylinder wall and piston. Assume that piston without damping hole, just consider this gap, According to the gap flow formula, the equation of pressure difference of hydraulic cylinder two cavity is:

$$p_{l2} = R_2 A_p \frac{dy_p}{dt} \tag{19}$$

Where R_2 is flowing resistance, $R_2 = \frac{12\mu l}{(1+1.5\varepsilon^2)\pi D_0 h^3}$; ε is relative rate of partial core, $\varepsilon = e/h$, e is eccentricity; h is gap width between cylinder wall and piston; D_o is diameter of piston.

The damping force of the gap effect is

$$F_2 = B_2 \frac{dy_p}{dt} \tag{20}$$

Where $B_2 = R_2 A_p^2$ is damping coefficient.

As a matter of fact, both damping hole and gap influence can be equivalent into a parallel circuit, that is,

$$p_{l1}=p_{l2}=p_l \qquad R_1q_1 = R_2q_2 \tag{21}$$

Therefore, $q = q_1 + q_2 = p_l\left(\frac{1}{R_1}+\frac{1}{R_2}\right)$,

so $p_l = \frac{R_1R_2}{R_1+R_2}q$.

Total damping force is

$$F = B\frac{dy_p}{dt} \tag{22}$$

Where $B=\left(\frac{R_1R_2}{R_1+R_2}\right)A_p^{\ 2}$ is total damping coefficient.

Assuming that the gap minimum, so $R_2 \gg R_1$, then $\left(\frac{R_2}{R_1+R_2}\right)\to 1$, that is $B \to B_1$.

Therefore, Total damping force is

$$F \approx B_1\frac{dy}{dt} \tag{23}$$

Shifting yoke installs the oscillation cylinder with rigid connection, the force of shifting yoke is equivalent to centralize into hydraulic cylinder. The force balance equation for the cylinder barrel is

$$A_p(p_1-p_2) = m_t\frac{d^2y_p}{dt^2} + B\frac{dy_p}{dt} + K_ly_p + F_l \tag{24}$$

Where m_t is equivalent mass; B is equivalent viscous damping coefficient; K_l is equivalent stiffness of spring; F_l is arbitrary load force on cylinder.

5 Analysis of vibration waveform

Solving mathematical models in the Simulink can obtained output curves of vibration waveform. The amplitude and acceleration of the excitation cylinder is considered as the main target.

The original position of the cylinder barrel is assumed as the origin of coordinates and forward direction is to the right. It is seen in Figure 8 that the period and displacement of the excitation cylinder, when the rotary frequency of spool is set to 5Hz (excitation frequency is 20Hz), are 2 times the size of that when the rotary frequency of spool is set to 10Hz (excitation frequency is 40Hz). Likewise, the period and displacement of the excitation cylinder, when the excitation frequency is 80Hz, are 1/2 times the size of that when the excitation frequency is 40HZ. The bigger the excitation frequency, the smaller the displacement of the excitation cylinder and the period of motion of y_p. When the valve orifice becomes wide, the right chamber of cylinder lets in the oil and left chamber drains the oil. As a result, the cylinder barrel moves right and gets the positive displacement. When we change the valve communication direction by rotating valve spool, the cylinder barrel moves left to the original position and keeps the displacement positive. Reciprocating motion of cylinder barrel is achieved by valve spool rotation.

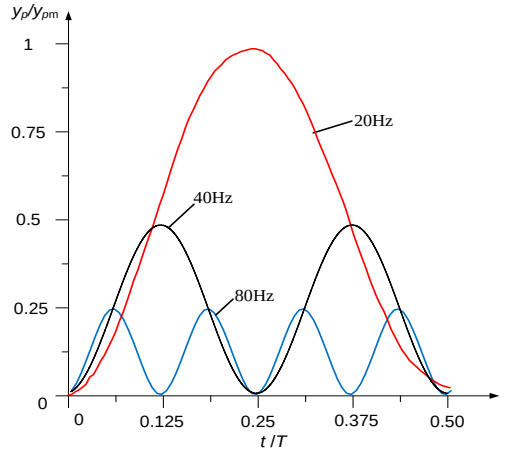

Figure 8 Curves of y_p- t with different frequency under no damping hole

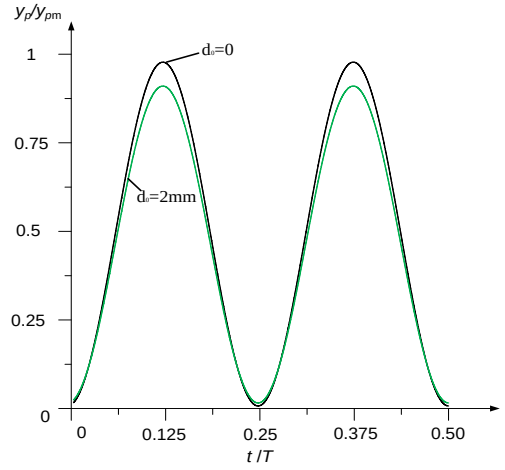

Figure 9 Curves of y_p- t with different d0

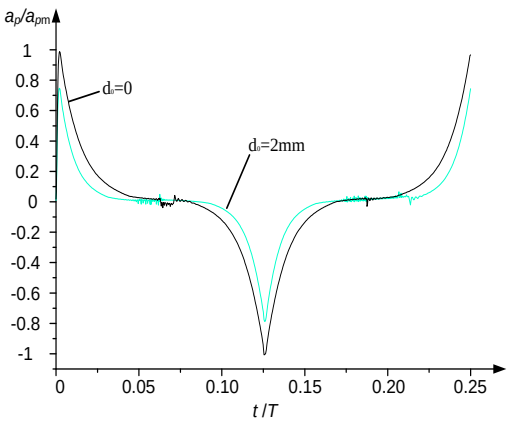

Figure 10 Curves of a_p- t with different d0

It is seen in Figure 9 and Figure 10, when f_1 and d_0 are given as 40 Hz, 2mm, the values of y_p and a_p is smaller than the one under no damping hole. Furthermore, y_p and a_p vary according to the value of d_0.

6 Experiments and discussion

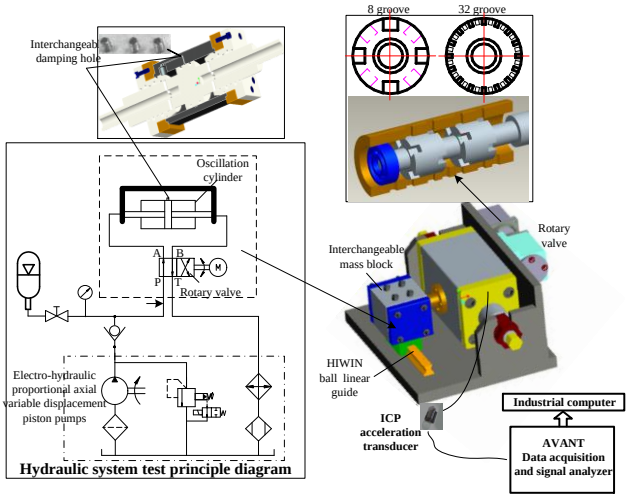

(a) System configuration

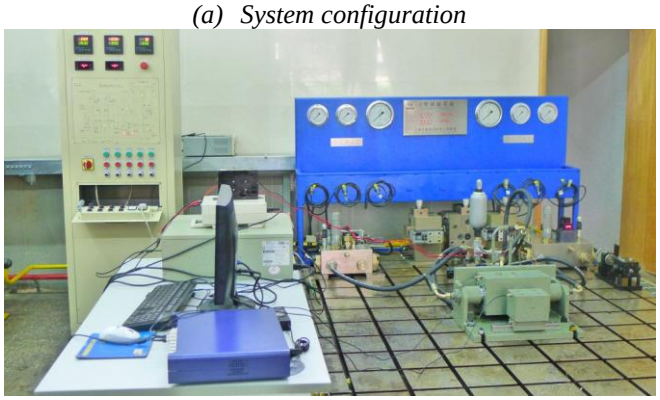

(b) Experiment test

Figure 11 Experiment system of the electro-hydraulic vibrator

The experiment system configuration of electro-hydraulic vibrator controlled by spin valve for tamping device is shown in Figure 11. The rotary motion of the valve's spool is driven by stepper motor. Interchangeable mass block on HIWIN ball linear guide is the equivalent mass of lower tamping arm. An ICP acceleration transducer was mounted outside the cylinder barrel to measure the acceleration of the cylinder barrel. The acceleration signals are acquired by AVANT and then are sent to industrial computer. AVANT Data acquisition and signal analyser is an integrated solution for dynamic signal analysis of vibration. It is designed based on distributed processing structure, integrating the up-to-date technology of multi-DSPs computation, vibration control algorithms and data transmission. Its USB2.0 connectivity ensures easy PC connectivity and high-speed disk throughout. AVANT possess functions of integral, quadratic integral and differential and so on. According to the acquired acceleration by accelerometer, the corresponding values of velocity and displacement will be easy to get. The main parameters of the vibrator structure and the hydraulic system are shown in Table 2.

Table 2 Main parameters of the vibration exciter

Item	Value
Maximum radial opening of the spin valve	6 mm
Maximum axial opening of the spin valve	6 mm
Spool Radius of the spin valve	15.5 mm
Number of grooves on a single spool	8
Diameter of the cylinder	100 mm
Diameter of the piston rod	70 mm
Volumer of the cylinder	$2.9\times10^{-4}m^3$
Interchangeable mass block	16~42kg
System maximum pressure	10 MPa
Maximum flow	100L/min
Natural frequency	267 HZ
Maximum hydrostatic force	40 KN

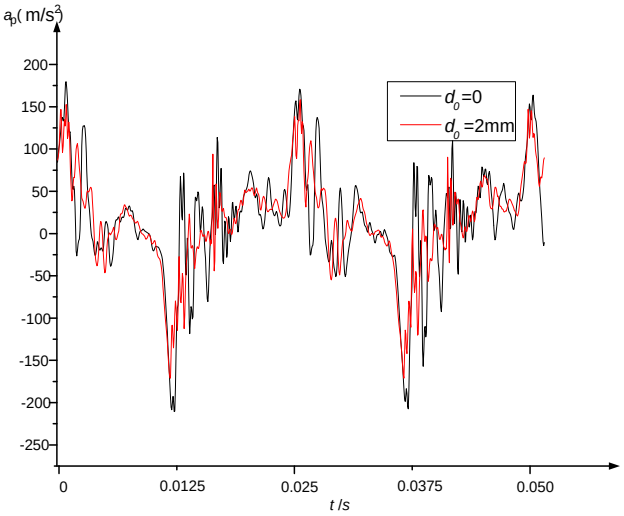

Figure 12 Curves of a_p- t with different d_0

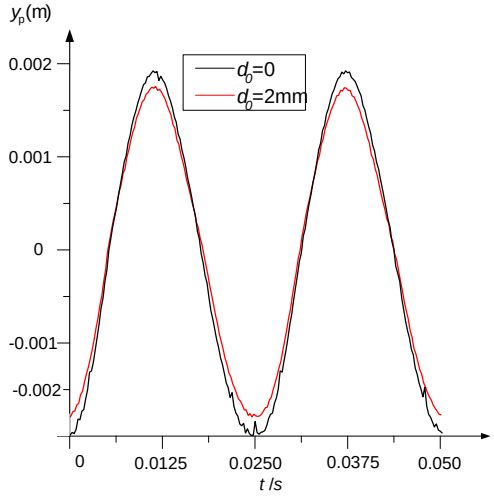

Figure 13 Curves of y_p- t with different d_0

When n, d_0, x_v and y_v are set to 600rpm, 0, 6mm, 6mm respectively, the maximal displacement and acceleration of the actuator can reach 4mm and 210 m/s^2 as is shown in Figure 12 and 13. The proportion of the above part and under part of the arm for the new tamping machine is

1:2.1 in terms of design length. Finally, the displacement 8mm and the frequency 40Hz of the tamping end are gotten. When d_0 are given as 2mm, the maximal value of y_p and a_p can get to 3.6mm, 180m/s^2 respectively. The maximal values under this condition is smaller than the one under no damping hole. The fluctuate value of a_p under this condition is also smaller than the one under no damping hole.The Curve of y_p under this condition is more smooth than the one under no damping hole. Furthermore, y_p and a_p vary according to the value of d_0. The result show that increasing hydraulic damping through the interchangeable damping hole can improve the vibration system performance.

7 Conclusion

1) A new tamping device with a hydraulic excitation and independent clamping movement is firstly proposed. It can overcome maintenance difficulty resulting from common shock mechanism and swing problem of the clamping hydraulic cylinder caused by tamping bar vibration. With the new working principle, A new spin valve is designed in order to fulfill dynamic state requirements of the oscillation cylinder.

2) The maximum displacement of the excitation cylinder is 4mm when the rotary spool frequency, the axial area gradient of valve port and the maximum radial guided width of the spool groove are set to 10Hz, 6mm and 6mm respectively. Finally, the vibration of the tamping bar, with the displacement being 8mm and excitation frequency 40Hz, can be achieved. It meets the design requirement. y_p and a_p vary according to the value of d_0. The experimental result show that increasing hydraulic damping through the interchangeable damping hole can improve the vibration system performance.

3) Under the different rotary spool frequency, the size and the changing period of the displacement of the excitation cylinder are different. The bigger the excitation frequency, the smaller the displacement of the excitation cylinder and the changing period of the displacement. As vibration with high frequency and low amplitude is fit for hardened ballast and vibration with low frequency and high amplitude is fit for loose ballast, through setting suitable related parameters in the electrohydraulic exciter, the new tamping device can satisfy all kinds of complex working environment.

4) Ballast characteristics are quite complicated and can not always be seen as invariable. Further research on this project will be conducted by taking into account of uncertain geological conditions and nonlinearities of ballast dynamics and electro-hydraulic system encountered in the tamping process.

8 References

[1] Cheng Wenming, "A Retrospect of the Development of Mechanical Equipments for Railway Maintenance in China," Modern Management, 2006(10). (in Chinese)

[2] Kou C Q, Zhou H L. Machinery on Railway Construction. Beijing: Machinery Industry Press, 2001. (in Chinese)

[3] Ying Lijun, Zhou Shuwu, Qi Lin, "Development of the Electric Recovery System of the 08-32 Tamper," Journal of the China Railway Society, 26(6). (in Chinese)

[4] Min Chaoqing, Gong Guofang, Liu Yi, "Design and Simulation Research on New Tamper Based on ADAMS," 2010International Conference on Digital Manufacturing & Automation(ICDMA 2010), IEEE Press, Dec, 2010, pp. 494-498.

[5] E Mark Rand, "Effect of Vibration on Ballast," Magazine of British Geography, 1981(09).

[6] HARSCO TECHNOLOGIES CORP (US) . Split tool tamper[P] .EP1172480， 2002.01.16 .

[7] HARSCO TECHNOLOGIES CORP (US) . Single shaft tamper with reciprocating rotational output[P].US6386114，2002.05.14 .

[8] HARSCO CORP (US) . Split tool tamper[P].DE60125871D，2007.02.22.

[9] MATISA MATERIEL IND SA(CH).Railway track ballast tamping device[P]. DE3165697D， 1984.09.27.

[10] MATISA MATERIEL IND SA (CH) . Railway track tamping device[P]. EP0050889，1982.05.05.

[11] MATISA MATERIEL IND SA . Railway ballast tamping machine[P]. EP0424322A1，1991.04.24 .

[12] PLASSER BAHNBAUMASCH FRANZ (AT) .Tamping machine for tamping ballast under the sleepers of a railway track[P]. EP1070787, 2001.01.24.

[13] FRANZ PLASSER BR BAHNBAUMASCHI (AT). Railway track tamping device and method[P]. EP1162309，2001.12.12.

[14] FRANZ PLASSERBAHNBAU MASCHINEN (AT) .Ballast Tamping Machine and Method for Tamping a Railway Track[P] . EP1403433 ， 2004.03.31.

[15] Sandsted C A, Moore M J, Delucia A P, et al. Split tool mechanical vibrator:US, 5584248[P]. 1996-12-17

[16] John M, Peter Y, Single shaft tamper with reciprocating rotational output: US, 6386114[P].2002-05-14

[17] Merritt H E. Hydraulic Control Systems[M]. New York: John Wiley & Sons, 1967.